Wear 610 (2027) 207197

Contents lists available at ScienceDirect

Wear

journal homepage: www.elsevier.com/locate/wear

Ultrasonic cavitation erosion in different biopolymer mixtures using deep eutectic solvents

Andraž Zupanc [a], Filipa A. Vicente [b], Matevž Dular [a], Marko Hočevar [a], Matej Hočevar [c], Odon Planinšek [d], Mojca Zupanc [a], Martin Petkovšek [a,*]

[a] University of Ljubljana, Faculty of Mechanical Engineering, Aškerčeva Cesta 6, 1000, Ljubljana, Slovenia
[b] National Institute of Chemistry, Department of Catalysis and Chemical Reaction Engineering, Hajdrihova 19, 1000, Ljubljana, Slovenia
[c] Institute of Metals and Technology, Lepi Pot 11, Ljubljana, Slovenia
[d] University of Ljubljana, Faculty of Pharmacy, Aškerčeva Cesta 7, 1000, Ljubljana, Slovenia

ARTICLE INFO

Keywords:
Cavitation mechanical effects
Chitin
Chitosan
Deep eutectic solvent
Aluminum specimen

ABSTRACT

Cavitation erosion is widely used to assess the mechanical effects of cavitation, but its interpretation becomes more complex in chemically reactive liquids. This study investigated ultrasonic cavitation in aqueous chitosan samples and chitin-containing deep eutectic solvent (DES) media using cavitation erosion on aluminum specimens as a quantitative probe. Cavitation was generated using a 20 kHz ultrasonic horn operating at a tip peak-to-peak oscillation amplitude of 50 μm and a 2 mm stand-off distance. The investigated media included Milli-Q water, chitosan suspensions, solutions and gels, and hydrated chitin-containing DESs based on choline chloride with malic or acetic acid. Material degradation was evaluated using cumulative mass loss measurements, 3D optical topography and scanning electron microscopy (SEM), while high-speed imaging was used to visualize cavitation dynamics. Density, surface tension, viscosity (unavailable for DES media), and vapor pressure were determined to relate erosion behavior to the physicochemical properties of the liquid media. Water-based media produced relatively low and spatially localized material loss, whereas hydrated DES media caused 49 times greater aluminum degradation and exhibited distinctly different cavitation dynamics. DES with acetic acid generated the most spatially developed cavitation cloud and, with chitin, produced the highest mass loss (49 mg after 60 min). Non-cavitated DES controls nevertheless showed measurable aluminum dissolution, confirming the contribution of chemical degradation. SEM and 3D topography revealed severe surface disruption within and beyond the horn footprint. Together, these findings demonstrate that mass loss in chemically reactive media reflects cavitation-assisted material degradation involving coupled mechanical and chemical effects.

1. Introduction

Acoustic cavitation generated by high-intensity ultrasound is a physical phenomenon involving the nucleation, growth and violent collapse of gas or vapor bubbles in a liquid medium subjected to alternating pressure fluctuations [1]. The implosive collapse of these bubbles releases energy within extremely confined area in space and time resulting in the mechanical and chemical phenomena associated with cavitation [2]. These include local hot spots [3], local shear forces [4], microstreaming [5], shock waves [6], microjets [7] and formation of reactive species [8]. Among the most prominent manifestations of mechanical effects of cavitation is cavitation erosion, defined as the progressive surface degradation of solids exposed to repeated bubble collapse events in their vicinity [6]. When bubbles collapse near a solid boundary, microjets and pressure pulses impact the surface, causing localized plastic deformation, pitting and ultimately material removal [9], [10]. Due to its sensitivity to cavitation intensity, cavitation erosion has been widely used as an indirect, yet quantitative, probe of cavitation activity in ultrasonic systems [11], [12], [13]. The ultrasonic vibratory method, standardized in ASTM G32 test, is commonly applied to study cavitation erosion under well-controlled laboratory conditions. In such configurations, erosion is typically quantified by monitoring mass loss over time and by surface characterization (e.g., microscopy or profilometry). Aluminum and its alloys are frequently used as model materials due to their relatively low cavitation resistance and reproducible erosion behavior [12], [14], [15]. Previous studies have demonstrated that

* Corresponding author.
E-mail address: martin.petkovsek@fs.uni-lj.si (M. Petkovšek).

https://doi.org/10.1016/j.wear.2026.207197
Received 1 September 2026; Received in revised form 20 November 2026; Accepted 23 November 2026
Available online 23 November 2026
0043-1648/© 2026 The Authors. Published by Elsevier B.V. This is an open access article under the CC BY license (http://creativecommons.org/licenses/by/4.0/).

erosion rates strongly depend on acoustic parameters such as amplitude, frequency and the distance between the sonotrode and the specimen [12], [13], [14]. Beyond acoustic parameters, the composition and rheological properties of the liquid phase decisively influence cavitation dynamics. Density, viscosity, surface tension, vapor pressure, and dissolved or dispersed species can influence bubble nucleation, growth and collapse vigor, ultimately affecting mechanical and chemical cavitation effects [16], [17], [18], [19]. While cavitation erosion in simple fluids such as water has been extensively investigated, considerably less attention has been devoted to cavitation behavior in more complex media, particularly those containing biopolymers or non-conventional solvents.

In recent years, cavitation has been increasingly applied in the processing of chitosan and chitin, two structurally related biopolymers derived from renewable biomass [20], [21], [22]. In aqueous chitosan samples, cavitation is known to induce chain scission, reduce molecular weight and decrease viscosity [21], [23], [24]. Several studies have shown that cavitation can facilitate the cleavage of 1,4-glycosidic bonds in chitosan through mechanical and/or chemical effects [21], [24], [25], [26]. At the same time, polymer chains alter the liquids viscoelastic properties, which can, in turn, modify cavitation dynamics [27], [28]. For chitin, which exhibits a highly crystalline structure and strong intermolecular hydrogen bonding, deep eutectic solvents (DES) have emerged as promising green alternatives to conventional harsh chemical treatments [22], [29]. DES are defined as a mixture of pure compounds, namely Lewis or Brønsted acids and bases, displaying a small difference in their acid-base strength, in which one compound acts as a hydrogen bond acceptor (HBA) and the other as a hydrogen bond donor (HBD), and for which the eutectic temperature is significantly depressed relative to the ideal mixture [30], [31]. DES can partially dissolve or swell chitin by disrupting its hydrogen bonded network while largely preserving its chemical integrity [32]. Their application in chitin extraction, dissolution and structural modification has been widely reported [22], [29], [33]. However, DES are typically highly viscous, exhibit extensive hydrogen bonding networks and reduced vapor pressure, all of which can influence cavitation behavior and energy dissipation during ultrasonication. The addition of water can substantially modify the intermolecular organization and physicochemical properties of DESs by altering HBA-HBD and ion-ion interactions, with the extent of these changes depending on both water content and DES composition. In particular, high viscosity and dense hydrogen bonding suppress bubble growth and alter collapse modes, while reduced vapor pressure affects nucleation thresholds and energy focusing during collapse, leading to cavitation regimes that differ fundamentally from those in aqueous samples [34].

Despite extensive research on both cavitation erosion and ultrasonic processing of chitin and chitosan, a systematic link between the properties of biopolymer containing media, cavitation dynamics, and the resulting mechanical impact on solid surfaces remains largely unexplored [27], [35], [36]. In particular, the use of cavitation erosion to assess how different liquids modulate cavitation intensity offers a valuable, yet underutilized approach for understanding and controlling ultrasound induced effects.

In this work, cavitation erosion generated by an ultrasonic probe was investigated using an aluminum specimen positioned beneath the ultrasonic horn tip in (i) MilliQ (MQ) water as a reference medium, ii) aqueous chitosan samples and (iii) chitin containing DES samples. The DES used in this study were selected based on [29], where they were identified as the most promising for chitin deacetylation. Cavitation-assisted material degradation effects were quantified by measuring time dependent mass loss of the aluminum specimen and analyzing changes in surface topography using non-contact optical microscopy - 3D profilometer and Scanning Electron Microscope (SEM), respectively. In order to support the interpretation of degradation behavior, selected physicochemical properties of the investigated media, including density, surface tension, viscosity, vapor pressure, particle size distribution and apparent contact angle (ACA) were measured. In addition, high-speed imaging of cavitation dynamics from side and bottom view supports the understanding of different erosion intensities. The novelty of this study lies in combining gravimetric measurements, surface characterization and high-speed visualization from two perspectives to investigate the cavitation-induced material degradation in complex liquid media. By relating the observed cavitation structures and physicochemical properties to changes in specimen mass and surface morphology, the study provides insights into the influence of medium composition on cavitation behavior and material degradation. The demonstration on how the physicochemical properties of the medium influence the mechanical effects of cavitation improve the understanding of ultrasonic processing of biopolymer samples. Furthermore, the study shows that special attention is needed when investigating cavitation erosion in hydrated DES media on aluminum specimens.

2. Materials and methods

2.1. Materials

Aluminum specimens (3.2 cm × 3.2 cm x 1 cm) were cut from 5083 aluminum alloy plate. Chitin and chitosan were supplied by Glentham Life Sciences (UK), with volume-weighted mean diameters D [3,4] values of 269.3 and 44.5 μm and surface area-weighted mean diameters D [2,3] values of 113.3 and 25.4 μm, respectively. The chitosan had a degree of deacetylation of 90.6%, weight average molecular weight (M_w) of 710 kDa and a dispersity ($Đ$) of 1.67 as determined by SEC-MALS-RI [21]. Acetic acid (AA) (>99.8%) was purchased from Honeywell Fluka. Choline chloride ([Ch]Cl), malic acid (MA) (99%) and H_2O_2 (34.5-36.5%) were supplied by Sigma-Aldrich. Sodium hydroxide pellets were obtained from Supelco.

2.2. Cavitation set-up

Cavitation was generated using ultrasonic horn – UH (UIP1000hdT, Hielscher Ultrasonics) ((1) in Fig. 1a) equipped with a titanium tip of 15.9 mm in diameter. Ultrasound was applied at a frequency of 20 kHz with the amplitude set to 100%, corresponding to a peak-to-peak tip oscillation amplitude of 50 μm. The UH tip was immersed in a 600 mL glass beaker (2) and positioned 2 mm above the square-shaped aluminum specimen (5), which served as an erosion indicator and was held by a holder (6) at a constant position. Deviation from standard ASTM G32 conditions was due to larger chitin particles. Temperature control was achieved using a submerged cooling coil (3) surrounding the UH, which was connected to a recirculating chiller (DuraChill CA03 with cooling capacity of 1.28 kW). The temperature was monitored using a thermocouple temperature sensor (4) positioned at the edge of aluminum specimen. For experiments involving volatile compounds (AA) the cavitation setup was operated inside a fume hood.

2.3. Experimental design

The experimental design (overview in Table 1) aimed to determine how the composition of the medium influence cavitation dynamics and the resulting degradation of aluminum samples. Attention was given to distinguishing cavitation-induced mechanical effects from chemical degradation in the hydrated DES systems. To systematically explore these effects, a series of experiments were carried out using polysaccharides chitin and chitosan, with variations in concentration, sample preparation method and solvent type. The conditions for chitosan experiments were selected based on our previous work on low molecular weight chitosan preparation [21], where conditions for chitin experiments were chosen based on study of chitin deacetylation using DES [29]. Chitosan experiments (H1-H7) and chitin experiments (Z1-Z4) were performed alongside controls (C1-C6) to establish reliable

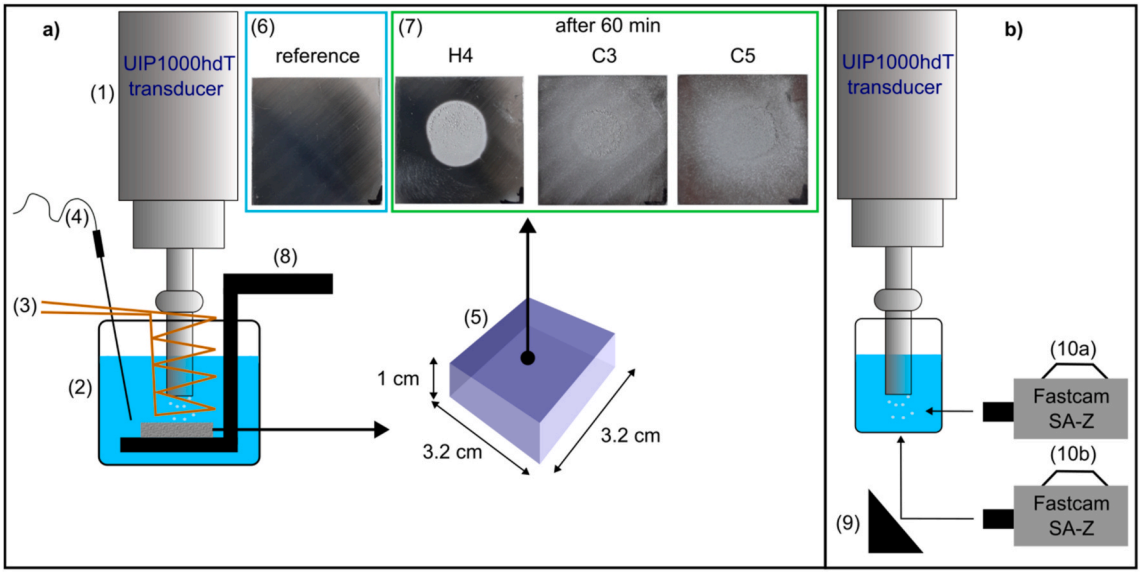


Fig. 1. a) Experimental set-up for erosion experiments: (1) ultrasonic horn, (2) glass beaker, (3) cooling coil, (4) temperature sensor, (5) enlarged view of the aluminum specimen with the surfaces shown in the (6) reference state and (7) after 60 min of cavitation for 3 example experiments, and (8) holder for the aluminum specimen. **b)** Visualization set-up: (9) mirror and (10a) high-speed camera position for side view and (10b) bottom view.

Table 1
Experimental design for the erosion experiments, including control (C1-C5), chitosan (H1-H7) and chitin experiments (Z1-Z4).

Exp.	Biopolymer	A [%]	c [g/L]	Medium	Mixture type	CH_3COOH addition	NaOH addition	Adjusted pH	H_2O_2 [g/L]
C1	/	100	/	MQ water	pure liquid	/	/	/	/
C2	/	/	/	[Ch]Cl:MA	solution	/	/	/	/
C2.1[a]	/	/	/	[Ch]Cl:MA	solution	/	/	/	/
C3	/	100	/	[Ch]Cl:MA	solution	/	/	/	/
C4	/	/	/	[Ch]Cl:AA	solution	/	/	/	/
C4.1[a]	/	/	/	[Ch]Cl:AA	solution	/	/	/	/
C5	/	100	/	[Ch]Cl:AA	solution	/	/	/	/
C6	/	/	/	MQ water	solution	/	/	/	3
H1	Chitosan	100	1	MQ water	suspension	no	no	7	/
H2	Chitosan	100	1	MQ water	solution	yes	no	4.4	/
H3	Chitosan	100	1	MQ water	gel	yes	yes	8.5	/
H4	Chitosan	100	1	MQ water	gel	no	yes	8.5	/
H5	Chitosan	100	1	MQ water	solution	yes	no	4.4	3
H6	Chitosan	100	1	MQ water	gel	yes	yes	8.5	3
H7	Chitosan	100	1	MQ water	gel	no	yes	8.5	3
Z1	Chitin	100	1	MQ water	suspension	/	/	/	/
Z2	Chitin	100	20	MQ water	suspension	/	/	/	/
Z3	Chitin	100	20	[Ch]Cl:MA	suspension[b]	/	/	/	/
Z4	Chitin	100	20	[Ch]Cl:AA	suspension[b]	/	/	/	/

A: UH amplitude.
[a] intense mixing without cavitation.
[b] dispersed and incompletely dissolved.

reference conditions. The study incorporated two biopolymer concentrations: 1 g/L (H1-H7, Z1), and 20 g/L (Z2-Z4). The chitosan sample preparation procedure included suspension (H1), dissolution (H2, H5) and gelation (H3, H4, H6, H7). In experiments H5-H7 H_2O_2 in concentration of 3 g/L was introduced as an oxidant, to assess whether oxidative conditions modify cavitation material degradation - erosion. MQ water served as a medium across the chitosan experiments (H1-H7), while chitin experiments were conducted in both MQ water (Z1, Z2) and DES (Z3, Z4). Control experiments with (C1, C3, C5) and without cavitation (C2, C2.1, C4, C4.1 and C6) were performed in pure liquids, to quantify media induced effects. All experiments were carried out at 23 ± 2 °C and medium volume of 333 mL.

For experiments conducted in MQ water, chitin and chitosan samples were freshly prepared prior to each erosion experiment to ensure reproducible physicochemical conditions. Chitin and chitosan suspensions were prepared by dispersing the respective biopolymer in MQ water (Table 1, Exps: H1, Z1, Z2). Chitosan solutions were prepared by acidifying chitosan suspension with AA to a final pH of 4.4, resulting in complete solubilization of chitosan (Table 1, Exps: H2, H5). Chitosan gels were prepared from either the corresponding suspension or solution by the addition of NaOH, which induced gelation. NaOH was added in the amounts sufficient to increase the pH of medium to 8.5 (Table 1, Exps: H3, H4, H6, H7). For experiments involving an oxidizing agent, H_2O_2 was added to the chitosan solution and gel immediately prior to the start of the experiment (Table 1, Exps: H5-H7). Sample pH was measured by HQ430d with PHC725 pH probe (Hach).

Deep eutectic solvents [Ch]Cl:MA and [Ch]Cl:AA were prepared by mixing hydrogen bond acceptor (choline chloride) with the corresponding hydrogen bond donor (malic acid or acetic acid) in a 1:2 M ratio. The amount of water present in each compound was previously measured as stated in Ref. [29]. The compounds were mixed at room temperature until a homogeneous and clear liquid was formed. The

DES-based media were prepared as aqueous DES mixtures containing 70 wt% DES and 30 wt% MQ water. The 70 wt% DES/30 wt% water composition was selected based on previous findings for [Ch]Cl:AA, this composition was identified as the most promising for chitin deacetylation, whereas for [Ch]Cl:MA, the addition of 30 wt% water reduced the viscosity to a level suitable for UH treatment. Chitin was dispersed in the DES at a concentration of 20 g/L (Table 1, Exps: Z3, Z4).

The nominal chloride content of the hydrated DES media was calculated from their composition, considering the 1:2 M ratio between [Ch]Cl and the corresponding acid, and the final water content of 30 wt %, according to Eq. (1).

$$b_{Cl^-} = \frac{0.70 \times 1000}{M_{[Ch]Cl} + 2M_{HBD}} \quad \text{Eq. (1)}$$

where b_{Cl^-} is the nominal chloride content (mol/kg of hydrated DES), 0.70 is the mass fraction of DES in the final mixture, 1000 is the conversion factor from kg to g, and $M_{[Ch]Cl}$ and M_{HBD} are the molar masses (g/mol) of choline chloride and the corresponding HBD, respectively. The factor of 2 accounts for the 1:2 M ratio between [Ch]Cl and the HBD. The calculation assumes 1 mol of chloride per mole of [Ch]Cl and represents the total nominal chloride content rather than the concentration of freely available chloride ions.

2.4. Characterization

2.4.1. Cavitation visualization

High-speed visualization was performed to compare the cavitation dynamics in the studied liquid media using a Photron FastCam SA-Z 2100K high-speed camera in 12-bit monochrome mode (Fig. 1b). At the side field of view the camera was positioned perpendicular to the UH axis operated at 80,000 fps with a resolution of 512 × 424 pixels. For a bottom field of view a mirror was installed below the glass container at 45° with camera's frame rate of 80,000 fps at 384 × 352 pixels. Shutter speed was set at 1 μs with medium open aperture on a Nikon 105 mm f/2.8G macro lens for both view positions. Side- and bottom-view recordings were acquired separately using the same high-speed camera.

2.4.2. Physicochemical properties of liquids

Physicochemical characterization of the investigated media was performed to relate the cavitation erosion behavior to the properties of the liquid phase and to better understand how medium composition influences cavitation-induced material wear. Density (ρ), surface tension (γ), viscosity (η), vapor pressure (p_v), particle size distribution and ACA measurements were therefore determined for the selected samples. To minimize temperature-related variations in the measured properties all measurements were performed under ambient temperature of 23 ± 2 °C unless stated otherwise. Each sample was measured in at least triplicate to ensure reproducibility. Density measurements were performed with standardized beam balance using the buoyancy (Archimedes') principle. The density of the liquid samples was determined by measuring the apparent mass change of a submerged reference body in the liquid, compared to its mass in air. Surface tension was measured using Tensiometer K12 (Krüss) employing the du Noüy ring method. Prior to each measurement, the platinum–iridium ring was thoroughly cleaned and flamed to remove any contaminants. The force required to detach the ring from the liquid surface was recorded and used to calculate the surface tension. Viscosity was measured using rotational rheometer Physica MCR 301 (Anton Paar). All viscosity measurements were performed defined shear conditions, while measurements in DES were not possible due to the equipment limitation, however the values for [Ch]Cl:MA are expected to be in the range between 1690 and 340 mPa s at 20 and 40% water, based on the literature [37]. Vapor pressure measurements were carried out using an in-house custom-built apparatus consisting of a closed bottle with a lid incorporating a temperature sensor and a port for controlled air evacuation. The sample was placed in the vessel in which pressure was lowered in a continuous and controlled way with a vacuum pump under controlled temperature conditions. The vapor pressure was determined at the boiling point under equilibrium conditions. Particle size distribution was measured using a Mastersizer 3000 (Malvern Panalytical) based on laser diffraction principle. Apparent contact angle between investigated media and virgin aluminum specimen was measured using DSA100 Drope Shape Analyzer (KRÜSS).

2.4.3. Erosion evaluation

Cavitation induced erosion of the aluminum specimens was quantified through mass loss measurements and surface topography analysis. The mass of the aluminum specimen was monitored throughout the erosion experiments using a PNJ 600-3M (Kern & Sohn) analytical balance with readability and reproducibility of 1 mg. This resolution allowed the observation of pronounced differences in cumulative material loss between aqueous and DES-based media. However, the relatively small mass losses measured in aqueous media were close to the balance readability and thus should be interpreted with caution, as their magnitude may be comparable to the weighing uncertainty. Erosion measurements were performed on a single aluminum specimen for each experiment (Table 1). Cumulative mass loss measurements were recorded at 8 sampling time points: 0, 1, 3, 5, 10, 15, 30 and 60 min, allowing evaluation of erosion kinetics over the full duration of each experiment. To minimize adhered deposits the following cleaning protocol was followed. After each exposure interval, the specimens were rinsed with Milli-Q water, dried with clean compressed air for at least 1 min followed by hot air, and cooled at ambient conditions for 30 min before weighing and later stored in a clean, dry container.

Surface morphology and topography were characterized using SEM and 3D optical Infinite Focus Measurement (IFM), respectively. SEM imaging was performed using an Apreo 2S LoVac SEM (Thermo Fisher Scientific) at 100× and 500× magnifications using Everhart-Thornley Detector (ETD) - emphasizing surface topography and Trinity T1 detector - emphasizing compositional contrast. Three-dimensional surface topography was measured using an InfiniteFocus G4 (Bruker Alicona) optical measurement system at 2.5x magnification with IF-MeasureSuite 5.1 software. Depending on the extent of the eroded area, up to a 4 x 5 matrix of individual fields was acquired and automatically stitched to obtain the complete surface topography. Alicona uses Focus-Variation to perform high resolution 3D surface measurements. A single aluminum specimen was investigated for each experimental condition. As independent experimental replicates were not performed, the results are presented without statistical error bars and should be interpreted as indicative trends rather than statistically validated differences between formulations.

3. Results

3.1. Cavitation visualization

Visualization of cavitation structures beneath the UH tip in investigated media is presented in Fig. 2 for the side view and in Fig. 3 for the bottom view with representative image sequences. Videos of both, side and bottom views are given in Supplementary Material (Suppl. S1).

In the side-view recordings, pure MQ water (C1) and chitosan solutions (H2 and H5) exhibited broadly similar cavitation structures. In these media, the cavitation cloud was concentrated toward the horn centerline and had a moderate axial extent. In contrast, the hydrated DES media C3 and C5 contained a visibly larger population of fine bubbles and fewer isolated large bubbles. The cavitation cloud in [Ch]Cl:AA (C5) appeared denser and extended farther in both the axial and lateral directions than that in [Ch]Cl:MA (C3). The standard-deviation maps calculated from the side-view sequences indicate the spatial region in which image intensity, and therefore cavitation activity, fluctuated during the recording. In C1, H2, and H5, the region of elevated

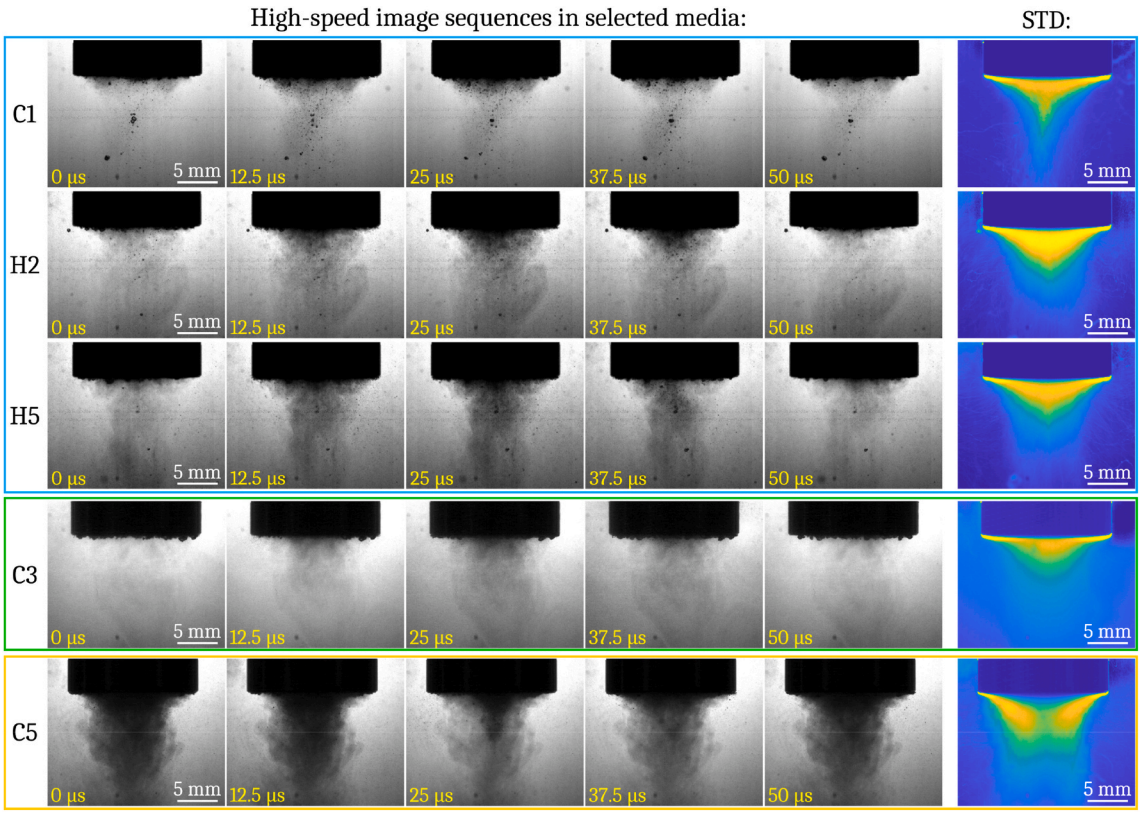


Fig. 2. Left side – Image sequence of cavitation under the UH tip in MQ water-based and both DES-based media from side view. Time step is written in yellow in bottom left corner of individual frame. Right side – Calculated standard deviation of cavitation appearance within 0.2 s long sequence, representing cavitation activity under the UH tip.

fluctuations was relatively narrow and centered beneath the horn. In case of hydrated DES media C5 resulted in most spatial distributed cavitation dynamics, while C3 shows least activities under the UH tip.

Bottom-view imaging (Fig. 3) demonstrates that cavitation is neither spatially nor temporally homogeneous across the UH tip but instead develops in localized regions of varying dynamics. The MQ water-based media (C1, H2, and H5) exhibit similar cavitation dynamics, characterized by a thin, highly dynamic cavitation layer composed of intermediate-sized bubbles that continuously expands, contracts, and reorganizes in response to the UH oscillation (in line with driving frequency of the UH). Larger bubbles are intermittently shed from the cavitation layer and propagate axially away from the horn. In contrast, the DES-based media (C3 and C5) display distinctly different cavitation regimes. Sample C3 forms a thinner cavitation layer consisting of apparently finer bubbles, with cavitation concentrated in localized regions that repeatedly collapse and reform, producing intermittent shedding of larger bubbles. Sample C5 differs most markedly from all investigated media, forming a dense cloud of fine cavitation bubbles that covers nearly the entire horn surface. The cavitation also spreads furthest beyond the horn perimeter, indicating the largest radial extent of cavitation structures within investigated media. Frequency spectra calculated from the bottom-view sequences showed a dominant response close to the 20 kHz driving frequency in all investigated media. A lower-frequency peak near 2.8 kHz was also observed, although its position varied moderately among the samples. In C5, additional spectral components near 17 and 22 kHz were detected. These additional components indicate more complex temporal modulation of the cavitation field in [Ch]Cl:AA; however, their precise physical origin was not determined in the present study.

3.2. Physicochemical properties

For each investigated liquid, characterization was performed with results presented in tabular form in Suppl. S2-S4, while only average values are reported in the main text. The density of the investigated aqueous chitosan-based samples remained close to that of MQ water. The reference sample C1 had a density of 0.9960 g/cm^3, while the chitosan samples H1–H7 ranged from 0.9959 to 0.9978 g/cm^3. This narrow range indicates that the preparation procedure, including suspension formation (H1), dissolution (H2, H5), gelation following dissolution (H3, H6) and gelation (H4, H7), had only a minor effect on the overall density. Although the addition of AA, NaOH, and H_2O_2 slightly changed the composition of the aqueous phase, these variations were not sufficient to cause pronounced density differences. The highest density among the chitosan samples was measured for H7, 0.9978 g/cm^3, but the value was still very close to that of MQ water. Therefore, the density of chitosan-based samples was governed mainly by the aqueous medium rather than by the mixture type of chitosan samples. Chitin suspensions in MQ water showed the same trend. Z1 and Z2 exhibited densities of 0.9964 and 0.9963 g/cm^3, respectively, despite the increase in chitin concentration from 1 to 20 g/L. This suggests that the dispersed chitin particles had a negligible influence on bulk density under the studied conditions. In contrast, the DES-based aqueous samples exhibited substantially higher densities, reaching 1.2460 g/cm^3 for Z3 in [Ch]Cl:MA and 1.0906 g/cm^3 for Z4 in [Ch]Cl:AA. These results demonstrate that density was primarily governed by the composition of the liquid medium, while the presence, concentration, and mixture type of the polysaccharide had only a limited effect in aqueous samples.

Compared with chitosan, chitin-containing samples showed a more pronounced decrease in surface tension compared to pure water (72 mN/m). Chitin MQ water suspension reduced the surface tension to 57.2 mN/m at 1 g/L (Z1) and further to 45.0 mN/m at 20 g/L (Z2),

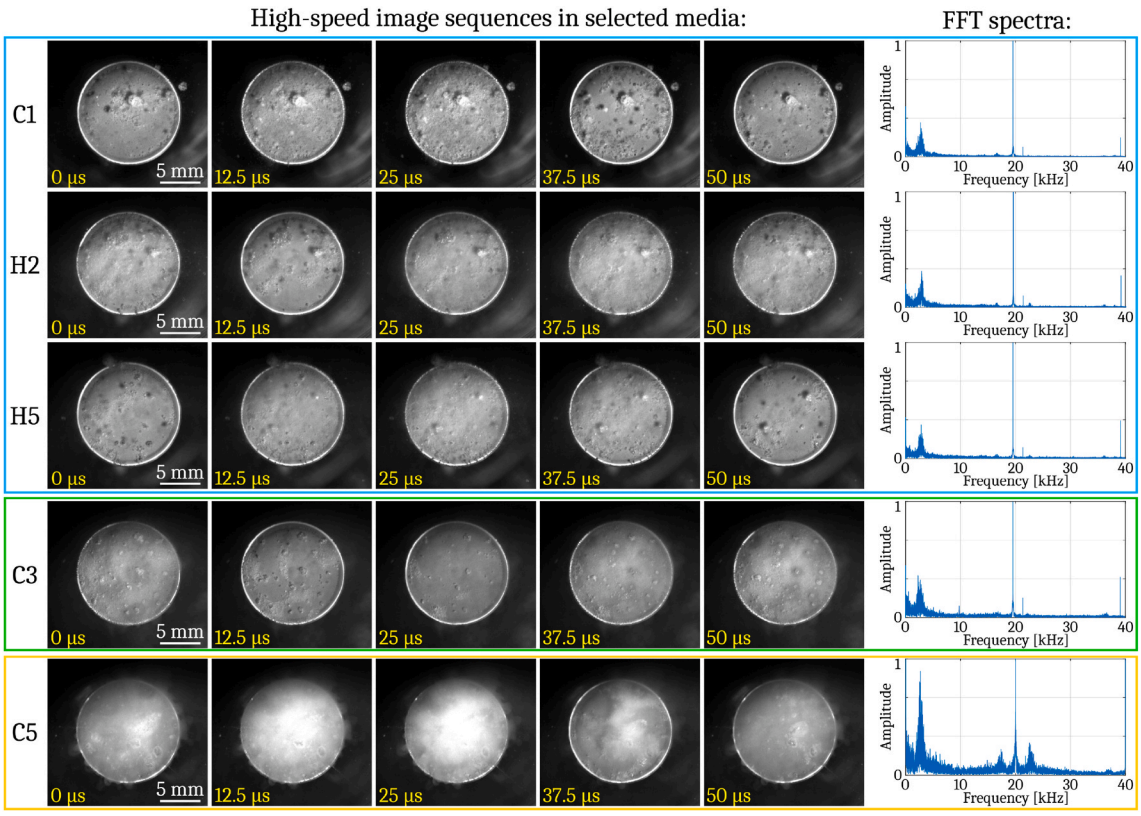


Fig. 3. Left side – Image sequence of cavitation under the UH tip in MQ water-based and both DES-based media from bottom view with glass bottom distanced 2 mm from the UH tip. Time step is written in yellow in bottom left corner of individual frame. Right side – Calculated Fourier transformation spectra of cavitation appearance within 0.2 s long sequence, representing cavitation frequency response under the UH tip.

despite the same aqueous medium, indicating an effect of chitin concentration. DES-based aqueous samples containing 30 wt% of water also exhibited reduced surface tension, with values of 47.3 mN/m for Z3 in [Ch]Cl:MA and 35.3 mN/m for Z4 in [Ch]Cl:AA. The lowest surface tension observed for Z4 indicates that the [Ch]Cl:AA-based medium had the strongest influence on the interfacial properties of the sample. Overall, the results show that surface tension was only slightly affected in most aqueous chitosan samples, whereas chitin concentration and especially the composition of the DES-based aqueous medium had a much stronger effect.

The apparent viscosity of chitosan-based samples was strongly influenced by the mixture type of chitosan. Samples were considered as Newtonian. The control sample C1 had a viscosity of 0.866 mPa s at 10 s^{-1}, while the chitosan suspension H1 showed a comparable value of 0.908 mPa s, indicating that suspended chitosan particles at 1 g/L had only a minor effect on bulk viscosity. In contrast, dissolved chitosan samples H2 and H5 exhibited markedly higher viscosities of 41.4 and 37.2 mPa s, respectively. This increase can be attributed to chitosan dissolution in acidic medium, where protonation of amino groups promotes polymer chain expansion and increases the hydrodynamic volume of the macromolecules, thereby enhancing resistance to flow [38]. The slightly lower viscosity of H5 compared with H2 may be related to partial oxidative degradation of chitosan in the presence of H_2O_2 [21]. Gelled chitosan samples showed considerably lower viscosities than the dissolved samples. H3, H4, H6, and H7 exhibited viscosities of 1.70, 0.926, 0.451, and 0.937 mPa s, respectively. The viscosity decrease after NaOH addition is consistent with deprotonation of chitosan amino groups and formation of heterogeneous gelled structures rather than homogeneous viscous solutions [21]. Overall, the results demonstrate that chitosan dissolution in acidic medium was the main factor responsible for the viscosity increase, whereas suspension formation and gelation resulted in viscosities close to that of the aqueous medium. The viscosity of the DES samples was not measured due to limitations of the rheometer device.

The MQ water had a vapor pressure of 2.90 kPa, while the chitosan samples H1-H7 showed values between 2.70 and 2.90 kPa. This narrow range indicates that the preparation procedure i.e., suspension (H1), dissolution (H2, H5), gelation following dissolution (H3, H6) and gelation (H4, H7) had only minor effect on the volatility of the aqueous phase. The lowest vapor pressure among chitosan samples was measured for H5, 2.70 kPa, which may be related to the presence of H_2O_2 and dissolved components in the acidic medium. However, the overall differences were small, indicating that vapor pressure was governed mainly by the aqueous medium rather than by the mixture type of chitosan. Aqueous chitin suspensions showed a similar behavior with Z1 and Z2 exhibiting vapor pressure of 2.91 and 2.98 kPa. In contrast, the DES-based samples exhibited markedly lower vapor pressure, with values of 1.57 kPa for Z3 in [Ch]Cl:MA and 1.76 kPa for Z4 in [Ch]Cl:AA. The lower vapor pressure of these samples could be attributed to strong interactions between water molecules and the DES, which reduce water activity and volatility compared to MQ water [39], [40]. Overall, vapor pressure was only slightly affected in the aqueous polysaccharide samples, whereas the composition of the DES-based aqueous medium had a much stronger influence.

Chitosan and chitin suspensions showed clearly different particle size distributions as shown in Suppls. S3 and S4. Chitosan particles were considerably smaller, with Dx(10), Dx(50), and Dx(90) values of 13.7, 37.9, and 86.3 µm, respectively (Suppl. S3). In comparison, chitin exhibited much larger particles, with corresponding values of 60.4, 229.3, and 537.7 µm. The median particle size of chitin was therefore approximately six times higher than that of chitosan. Moreover, the Dx (90)/Dx(10) ratio was lower for chitosan than for chitin, 6.3 and 8.9, respectively, indicating a narrower and more homogeneous size distribution for chitosan. The high Dx(90) value of chitin, exceeding 0.5 mm,

further suggests the presence of a coarse particle fraction. Overall, these results demonstrate that chitin suspensions contain larger and more broadly distributed particles than chitosan suspensions.

ACA measurements showed that the wettability of the virgin aluminum specimen surface depended strongly on the composition of the liquid medium. MQ water based media had an ACA of 86°, indicating relatively limited wetting of the aluminum surface. In comparison, the measured chitosan-based samples showed similar ACA values, ranging from 81° for H2 to 89° for H5. These results indicate that preparation procedure, including dissolution (H2, H5), gelation following dissolution (H3, H6) and gelation (H4, H7), had only a minor effect on the overall wetting behavior of the aqueous chitosan samples. In contrast, the DES-based samples showed markedly lower ACA values. The [Ch]Cl:MA (C3) had an ACA of 70°, while the [Ch]Cl:AA (C5) showed value of 52°. This indicates better wetting of the aluminum surface compared with MQ water and chitosan-based samples. The lower ACA value for [Ch]Cl:AA compared to [Ch]Cl:MA is consistent with higher aluminum mass loss observed in [Ch]Cl:AA. The nominal chloride contents of the hydrated DES media were 1.72 and 2.70 mol kg^{-1} for [Ch]Cl:MA and [Ch]Cl:AA, respectively. The higher chloride content in [Ch]Cl:AA results from the lower molar mass of acetic acid compared to malic acid, despite both DES having the same molar ratio and water content. The corresponding apparent pH values were 0.226 ± 0.019 and 1.540 ± 0.011 for [Ch]Cl:MA and [Ch]Cl:AA, respectively.

3.3. Erosion evaluation

The cumulative mass loss during cavitation erosion measured after 60 min is presented in Fig. 4, while the complete time-dependent dataset is provided in Suppl. S5. Cavitation erosion in pure water (C1), which served as a reference experiment, experienced the lowest wear in terms of mass loss (1 mg). MQ water-based media experiments (H1-H7, Z1-Z2) have a range of mass loss between 2 and 9 mg for all mixture types and both biopolymers. Highest mass losses were recorded using hydrated DES media (up to 49 mg).

The chitosan suspension H1 and the chitin suspension Z1 both produced a mass loss of 4 mg, despite the substantially smaller particles present in H1. Increasing the chitin concentration from 1 g L^{-1} in Z1 to 20 g L^{-1} in Z2 reduced the final mass loss slightly, from 4 to 3 mg. The chitosan solution H2 resulted in a mass loss of 3 mg. H3, in which chitosan was first dissolved and then gelled, resulted in 2 mg of mass loss, the lowest value among the chitosan-containing formulations. In contrast, H4, which was gelled without prior acidic dissolution, produced a mass loss of 6 mg. The addition of H_2O_2 increased mass loss in the formulations containing acetic acid. H5 and H6 both reached 9 mg, compared with 3 mg for H2 and 2 mg for H3 without H_2O_2. In contrast, H7 resulted in the same final mass loss as H4, 6 mg.

For DES-based aqueous media, the interpretation of mass loss must also consider the chemical dissolution of aluminum by the medium itself. Therefore, polymer-free DES-based samples were evaluated without cavitation in standing still liquid (C2 and C4) and intense mixing (C2.1 and C4.1) and under cavitation conditions (C3 and C5). In the absence of cavitation, [Ch]Cl:MA and [Ch]Cl:AA already caused measurable aluminum mass loss, reaching 6 mg and 5 mg for (C2) and (C4), respectively, after 60 min in still liquid, while with mixing the mass loss increased to 7 mg for both C2.1 and C4.1. This confirms that both hydrated DES media were chemically active towards aluminum and that the total mass loss in these samples cannot be attributed solely to mechanical cavitation erosion. Furthermore, the presence of cavitation substantially increased the mass loss reaching 18 and 34 mg in C3 and C5, respectively. For two different DES-based aqueous media one can see severe material loss, which peaks within [Ch]Cl:AA and presence of chitin particles (Z4) at 49 mg. The presence of chitin particles (Z4) indicates that solid particles extensively boost the erosion process in [Ch]Cl:AA, while another hydrated DES media [Ch]CL:MA showed even a slight decrease in mass loss when chitin particles were present (Z3) in comparison to pure [Ch]Cl:MA solution (C3), 18 mg compared to 16 mg, respectively. This suggests that, in the [Ch]Cl:MA aqueous medium, chitin did not intensify aluminum degradation, however due to relatively small measured difference in mass loss and lack of independent replicates, no firm conclusions could be made. Possible contributions from particle-induced bubble nucleation, changes in local cavitation dynamics, and mechanical interactions near the aluminum surface remain hypothetical and require further investigation.

Time dependent mass loss results (Fig. 5) reveal that mass loss rates differ between MQ water and DES-based media. While in case of MQ

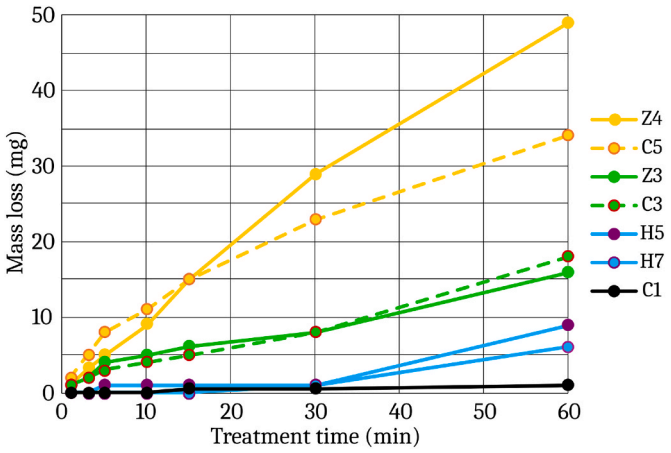


Fig. 5. Time dependent mass loss curves for control C1, chitosan solutions in water-based media H5 and H7 and both hydrated DES media with and without dissolved chitin.

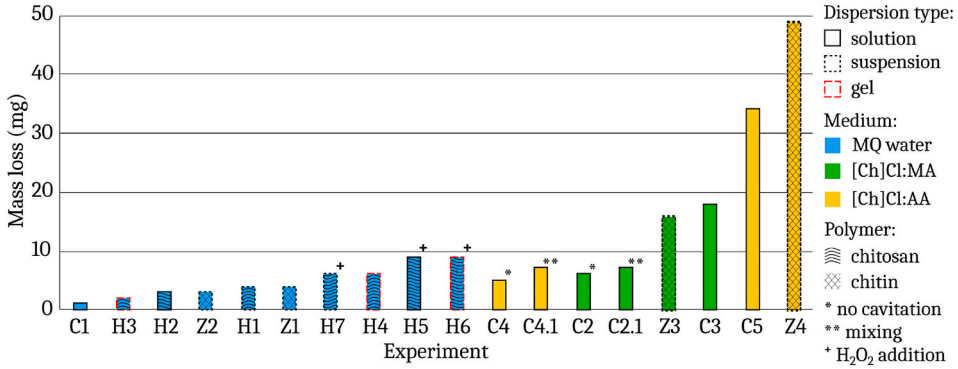


Fig. 4. Cumulative mass loss of all specimens after 60 min of treatment. Medium in which samples were prepared is marked with color, dispersion type is outlined with solid or dashed lines and presence of polymer is marked with a pattern.

water-based media (H5, H7) there is distinct incubation phase (up to 30 min treatment time), in DES-based media this period is extremely short, under 1 min, when first mass measurement took place. Also, between two selected hydrated DES media mass loss rates strongly differ, even though the control experiments without cavitation presence (C2 and C4) show similar dynamics (Suppl. S5), suggesting that cavitation intensity differs between selected DES media. The presence of chitin within [Ch]Cl:AA DES medium (Z4) increased material wear in presence of cavitation for over 30%. On the other side with [Ch]Cl:MA no significant change in the presence of biopolymer can be observed.

Topography analysis of the aluminum specimens revealed the extension of the erosion process under the UH tip after 60 min of treatment (Fig. 6 and Suppl. S6). Non-treated surface exposes the marks of aluminum alloy plate finishing process in the form of grooved pattern, which is intact outside of the eroded area under the UH tip in the case of aqueous media (Fig. 6 – C1, H2, H5). The hydrated DES media, as already mentioned, have chemical impact on the material itself, that can be seen as impacted surface outside of the near UH tip area, where no grooved pattern could be observed anymore (Fig. 6 – C3, Z3, C5, Z4). Yet the grooved pattern is still present at the control experiments without cavitation (C2, C2.1 and C4, C4.1), which indicates that the presence of cavitation is needed to erode the material severely. Even with intense mixing (C2.1 and C4.1) the pattern can still be noticed (Suppl. S6). Profiles at the bottom of the topography images (Fig. 6) show vertical and horizontal average profiles in the width of 1 mm across the center of the eroded area. C5 and Z4 exhibit the greatest material loss and the most pronounced surface damage. However, sample H5 also exhibits deep concave depressions and a high number of deep pits, similar to Z4, although the overall material loss is lower. This difference can be attributed to the fact that the entire surface of sample C5 was subjected to erosion, whereas in H5, erosion was primarily localized to the surface exposed to cavitation. Profiles support topography images, where surface roughness can be estimated and compared.

Figs. 7 and 8 show degradation morphology changes on aluminum specimen surfaces under different investigated conditions. The reference sample (Fig. 7) shows expected relatively smooth surface with pronounced parallel machining marks. Surfaces exposed to MQ water (C1) and water-based media (H6) within the UH area show severe modified surface. Case H6 resulted in stronger surface modifications in comparison with C1, which correspond to mass loss results. Region outside of UH area is unmodified and appears as original reference sample in all water-based experiments (example shown for case H6).

Fig. 8 presents morphology changes of surfaces exposed to [Ch]Cl:AA under different conditions. Exposure to [Ch]Cl:AA for 60 min without cavitation (C4) already resulted in morphology changes. Most of the original machining marks are not visible any more due to the corrosion process (white marks). With addition of mixing (C4.1) the surface modification became more spatially extensive and only isolated spots of original surface can be observed, which also supports mass loss results. By adding the effect of cavitation (C5) a severe change in form of pits can be observed, which corresponds to intense cavitation conditions. The surface (area directly exposed to cavitation) exhibits a strong irregular morphology with numerous pits and extensive roughness. All this corresponds well with mass loss measurement results: C4 – 5 mg, C4.1 – 7 mg and C5 – 34 mg.

Higher magnifications of case C5 reveal that in the area of UH tip, the surface was strongly modified by cavitation bubble collapses, while outside of the UH area angular and step-like shape features (Fig. 8. Exp. C5 - A) can be observed. Besides these features also clustered deposits of cauliflower-shapes (Fig. 8. Exp. C5 - B) can be observed, especially under T1 detector.

When chitin particles are added to the [Ch]Cl:AA medium (Z4), the surface roughness is even higher with deeper pits, corresponding to higher mass loss (49 mg) in comparison with the experiment without particles (C5 – 34 mg). Within the area directly beneath the UH (Fig. 8 third row), SEM revealed a highly irregular and strongly developed surface morphology characterized by extensive roughening, large irregular cavities (molten lava-like shapes seen on Fig. 8 third row C), and pronounced surface relief. At higher magnifications, angular and step-like features were observed together with fine clustered surface

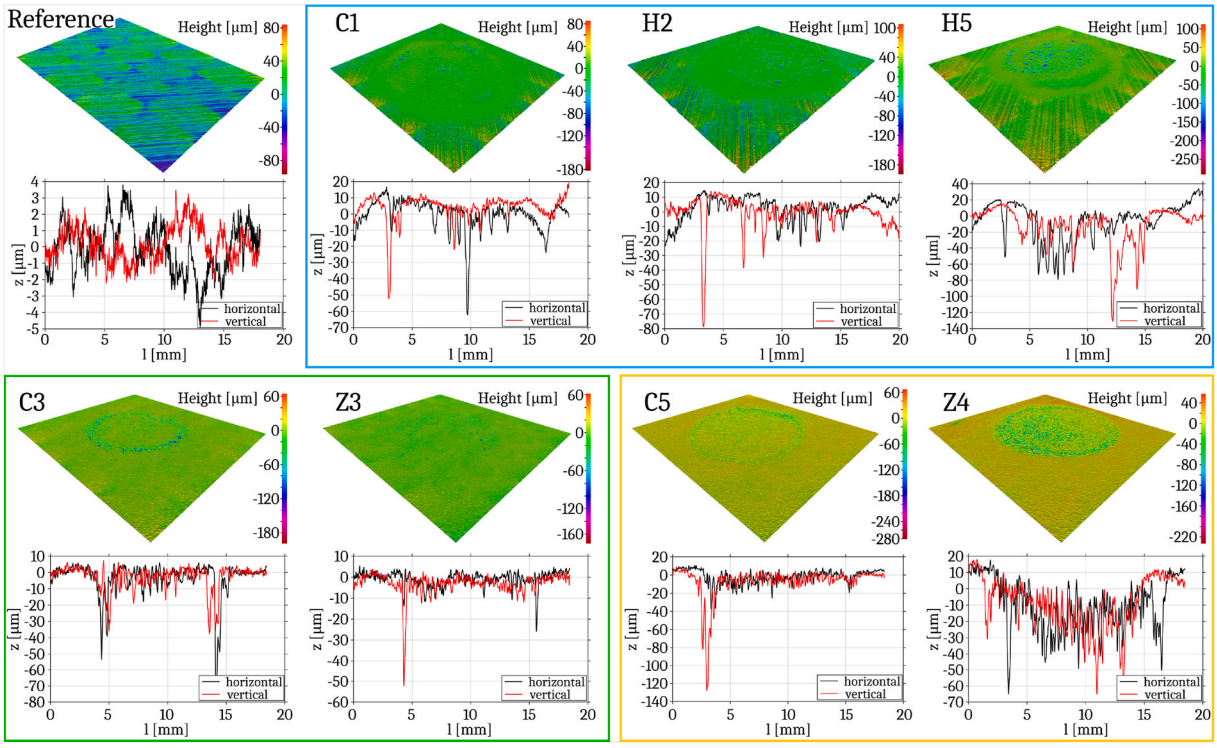


Fig. 6. 3D topography of the selected specimens after 60 min of treatment with corresponding line profiles with average 1 mm width in horizontal and vertical direction, respectively. Diagrams have individual color bar and z-scale range.

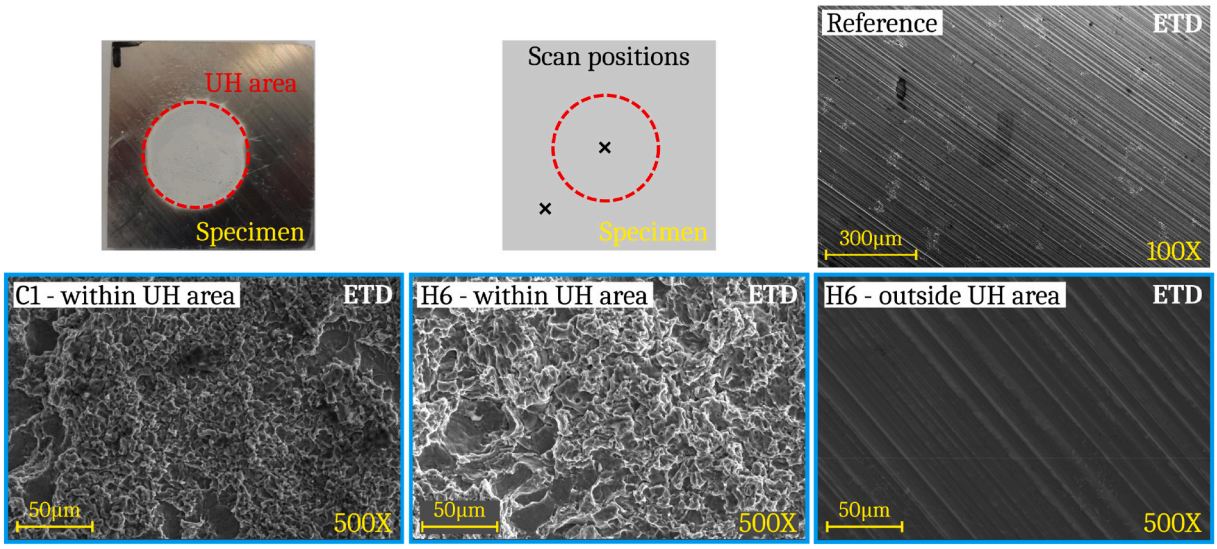


Fig. 7. SEM images of selected specimens after 60 min of treatment, captured with ETD detector. Upper left and center image presents eroded area and positions of SEM presenting and outside UH area. Upper right image shows reference surface prior cavitation exposure. In the right and left bottom corners of individual images magnifications and size markers are given in yellow.

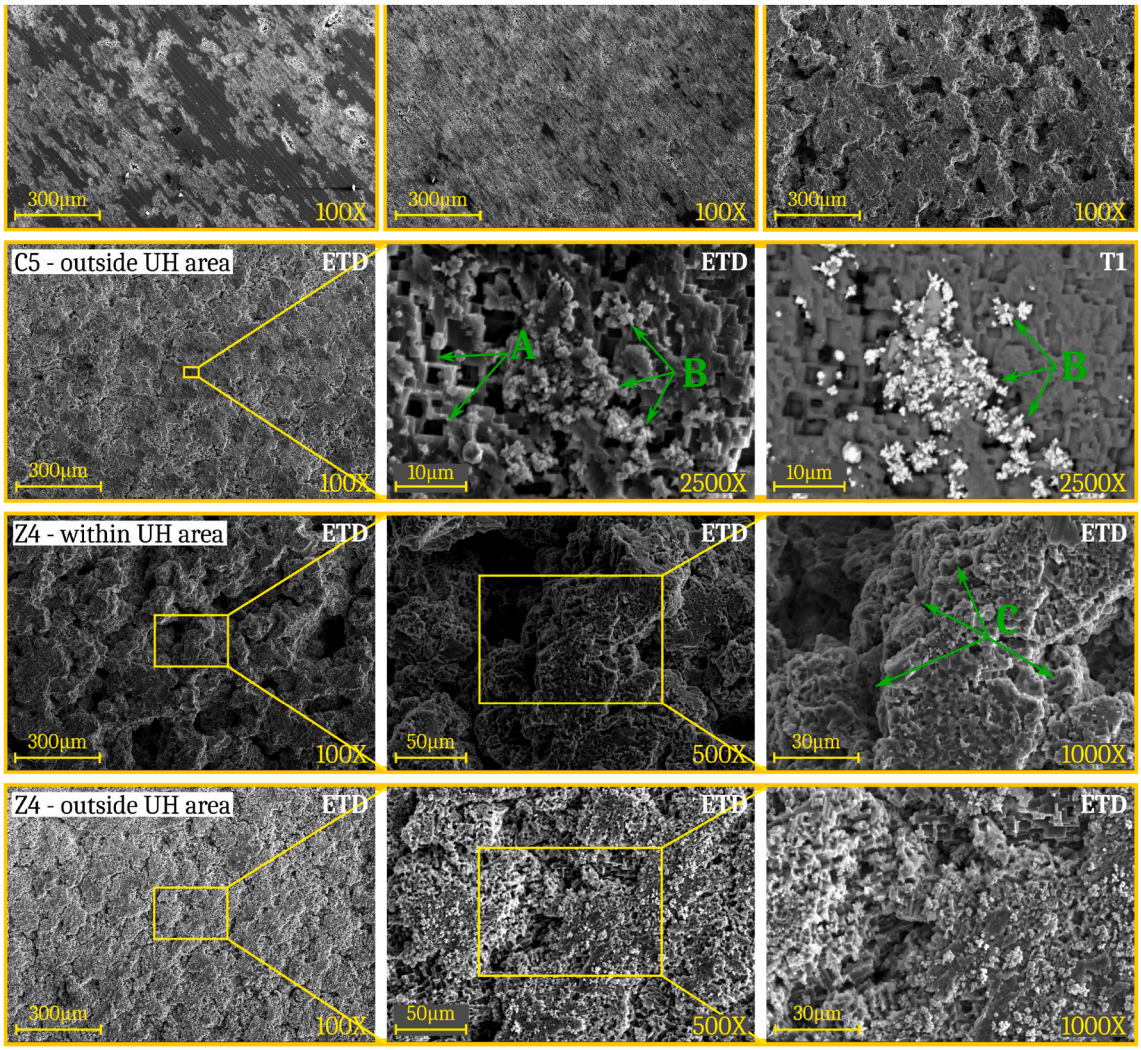


Fig. 8. SEM images of selected specimens after 60 min of treatment, captured with ETD and T1 detector. All images present surface morphology of specimens treated within [Ch]Cl:AA. Middle and bottom row are a series of same specimen with different magnifications within and outside UH area. In the right and left bottom corners of individual images magnifications and size markers are given in yellow.

deposits. Outside the UH area (Fig. 8 bottom row), surface degradation was less severe but remained extensive, with the original machining marks no longer visible. In contrast to the strongly disrupted morphology within the UH area, the outer region exhibited a more pronounced angular and step-like structure, including sharply defined cavities and numerous fine cauliflower-like surface features distributed extensively across the degraded surface.

4. Discussion

The combined high-speed imaging and erosion measurements demonstrate that medium composition substantially changed both cavitation dynamics and the resulting material wear on aluminum specimens. The aqueous samples produced cavitation fields broadly resembling that in MQ water, whereas the hydrated DES media generated denser populations of finer bubbles and a wider spatial distribution of activity. The most pronounced difference was observed in [Ch]Cl:AA, which formed the broadest and densest cavitation cloud and produced the greatest specimen mass loss. This confirms that cavitation in hydrated DES media occurred in a different regime than in water, most likely due to the altered physicochemical properties of the liquid phase (Suppl. S2), including lower surface tension, lower vapor pressure, and stronger intermolecular interactions [34], [40]. This observation is consistent with the higher mass loss measured in DES samples and supports the conclusion that [Ch]Cl:AA promoted more intense cavitation-assisted aluminum degradation than [Ch]Cl:MA. Interestingly, the non-cavitated controls showed comparable aluminum mass loss for the two hydrated DES media, both under static conditions and intense mixing. Therefore, the substantially higher mass loss observed for [Ch]Cl:AA under cavitation cannot be attributed solely to a greater chemical aggressiveness of this medium towards aluminum, but rather indicates an interplay between the chemical environment and cavitation dynamics. The high erosion observed for Z4 can therefore be attributed to the combined effects of the hydrated DES medium, the more developed cavitation cloud beneath the UH tip and potentially the presence of chitin particles, which would require additional tests to verify their contribution. However, the individual contributions of these factors could not be quantified in the present study.

The results further show that not a single physicochemical property (Fig. 9) can explain the overall observed material loss. Density varied only slightly among the aqueous samples, while considerably different mass losses were measured. Similarly, no clear relationship between apparent viscosity and mass loss was observed. A tendency toward increased mass loss at lower surface tension was apparent when the DES samples were included, but the aqueous chitin suspensions demonstrate that reduced surface tension alone was insufficient to produce severe aluminum specimen degradation. Likewise, the low vapor pressures of the hydrated DES media coincided with high mass loss, whereas the aqueous samples exhibited similar vapor pressures but different erosion responses. The physicochemical-property plots should therefore be interpreted as showing broad associations rather than independent causal relationships as cavitation behavior was governed by the combined effects of medium composition, interfacial properties, rheology, and dispersed phases.

In the aqueous samples, material removal remained relatively low and was mainly localized beneath the UH. The small decrease in mass loss observed when the chitin concentration was increased from 1 to 20 g/L (Z1 and Z2) may indicate partial attenuation of cavitation loading by the increased particle population. Bubble-particle interactions can modify bubble growth, collapse asymmetry, and micro-jet formation near solid boundaries [41]. However, the difference between Z1 and Z2 was small, and the present data does not provide sufficient evidence to establish a concentration-dependent protective effect.

The addition of H_2O_2 increased aluminum mass loss in the chitosan samples containing acetic acid, suggesting that oxidative processes may have contributed to material degradation in addition to mechanical cavitation erosion. Cavitation-induced microjets and shock waves can repeatedly disrupt the passive oxide layer on aluminum, exposing the underlying material and thereby facilitating corrosion. Such a synergistic interaction between cavitation erosion and corrosion has previously been demonstrated for aluminum alloys under cavitating conditions [15]. In the presence of H_2O_2, cavitation-generated reactive

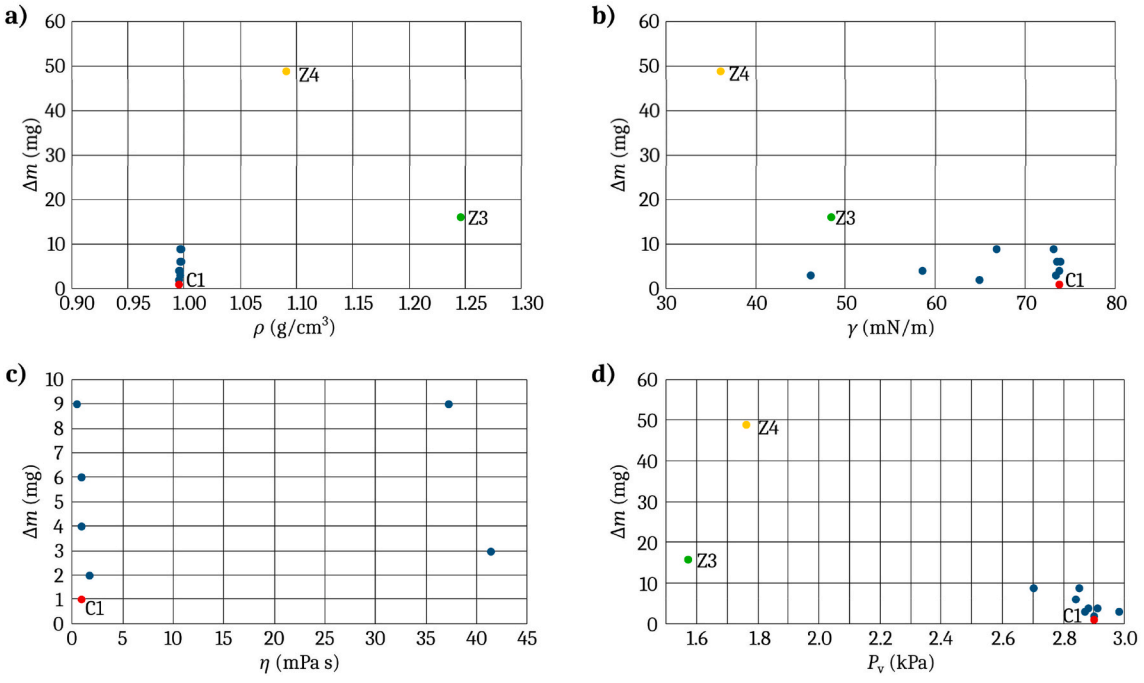


Fig. 9. Correlation between the cavitation erosion mass loss after 60 min (Δm) and the physicochemical properties of the tested formulations: a) density, b) surface tension, c) apparent viscosity, and d) vapor pressure. Red symbols indicate control C1, while yellow symbols indicate hydrated DES based samples Z3 and Z4. The complete dataset used for the correlation analysis is provided in Suppl. S2.

species may further promote oxidative surface degradation, however, the contribution of this mechanism cannot be distinguished from mechanical erosion based on the present mass-loss measurements alone. Nevertheless, H7 showed the same final mass loss as H4, indicating that the effect of H_2O_2 depended on the chitosan preparation route and formulation structure. Furthermore, the C6 control of H5 experiment (dissolved chitosan in the presence of H_2O_2), where sample was exposed to intense mixing without the cavitation for 60 min, showed no reduction in specimen mass.

The hydrated DES samples require a different interpretation because the non-cavitated controls have already caused measurable aluminum mass loss. Thus, total mass loss in C3, C5, Z3, and Z4 cannot be attributed solely to mechanical cavitation erosion. The chemical interaction of DES-based media with aluminum strongly depends on their composition, including the nature of the HBD, water content, acidity and chloride availability. In the present hydrated ChCl:carboxylic acid systems, the nominal chloride contents were calculated as 1.72 and 2.70 mol kg^{-1} for [Ch]Cl:MA and [Ch]Cl:AA, respectively, considering the 1:2 M ratio and 30 wt% water. The corresponding apparent pH values were 0.226 ± 0.019 and 1.540 ± 0.011, respectively. The acidic environment may contribute to the destabilization and dissolution of the protective aluminum oxide layer, while chloride-containing species may further assist metal dissolution through complexation and ligand-exchange processes. Previous studies have shown that proton activity and HBD coordination influence metal oxide dissolution in DES [42]. For aluminum systems, Ahmed et al. [43] also showed that the nature of the acidic HBD and the stability of the passive layer may play a more important role than chloride concentration alone. Similar effects on the removal of protective oxide layers have also been reported for stainless steel in hydrated DES [44]. Besides the chemical contribution, ultrasound can further accelerate material degradation through acoustic streaming, micro-mixing, repeated disruption of surface films, and enhanced transport of dissolved species. Ultrasound-assisted dissolution of metal oxides in DES has been previously reported by Gradov et al. [45], while Hunt et al. [46] demonstrated that ultrasound can reduce surface passivation and promote localized etching in DES-based electrochemical systems. Daskalopoulou et al. [47] also showed that ultrasound can enhance metal dissolution in dense ionic fluids through improved mass transport. In our experiments, passive exposure to hydrated DES media resulted in mass loss of 6 and 5 mg for C2 and C4, respectively, while intense mixing without cavitation increased these values only slightly to 7 mg in both cases (C2.1 and C4.1) after 60 min. Under cavitation, however, mass loss increased to 18 mg for C3 and 34 mg for C5. These results indicate that chemical interactions contribute to aluminum degradation, while cavitation substantially increases material loss through additional mechanical and transport effects.

The contrast between [Ch]Cl:MA and [Ch]Cl:AA was particularly pronounced. [Ch]Cl:AA produced substantially higher mass loss and a broader, denser cavitation cloud than [Ch]Cl:MA. The lower surface tension and apparent contact angle of [Ch]Cl:AA indicate different interfacial behavior and more effective wetting of the aluminum surface, while the high-speed recordings show that the cavitation field itself was also altered. The type of the hydrogen-bond donor is known to influence viscosity, polarity, conductivity, and intermolecular organization in choline chloride-carboxylic acid DESs [48]. In the present systems, the relatively high water content (30 wt%) should also be considered, as hydration modifies the HBA-HBD and ion-ion interactions characteristic of the neat DES and can substantially alter its physicochemical properties. These changes depend on the DES composition and may therefore differ between [Ch]Cl:MA and [Ch]Cl:AA. Consequently, the greater degradation in [Ch]Cl:AA most likely resulted from the combined effects of medium composition and structure, cavitation dynamics, interfacial wetting, and enhanced mass transport rather than from any single measured property.

The effect of chitin was also dependent on the surrounding DES. In [Ch]Cl:MA, the addition of chitin produced only a small decrease in mass loss relative to the polymer-free cavitated control, suggesting that chitin did not profoundly intensify degradation under these conditions. In contrast, chitin increased the mass loss in [Ch]Cl:AA from 34 to 49 mg. The dispersed and incompletely dissolved particles may have influenced bubble nucleation, altered the local cavitation field, or contributed to mechanical and/or chemical interactions near the aluminum surface. However, these mechanisms were not directly verified, and the absence of independent experimental replicates prevents definitive conclusions regarding the influence of chitin. Further experiments are required to establish whether the observed differences are reproducible.

The SEM observations of DES-based samples provide particularly strong evidence for the coexistence of mechanical and chemical degradation mechanisms. Within the UH area, the surface exhibited extensive relief, large irregular cavities, and highly disrupted morphology. Such features are consistent with intense localized loading caused by cavitation bubble collapse, superimposed on chemical attack by the DES medium. Outside the UH area, degradation was less severe but remained extensive. At higher magnification, this outer region displayed numerous sharply defined angular cavities, terrace-like stepped structures, and fine cauliflower-like deposits. The more regular angular morphology differs markedly from the strongly disrupted surface within the directly cavitated region and is consistent with preferential chemical dissolution of the alloy surface. Similar micro-step-like morphologies have been reported for chemically etched aluminum AA1050, where preferential attack at surface defects leads to pit formation and progressive development of a stepped microtexture [49]. The cauliflower-like structures are most reasonably interpreted as surface reaction or precipitation products. However, to identify specific composition of these deposits, additional characteristic methods would be needed. Cauliflower-shaped morphologies have previously been reported in corrosion-damaged metallic surfaces and associated with pitting corrosion [50]. Moreover, aluminum has been shown to undergo electrochemical dissolution and subsequent deposition from DES-based electrolytes, producing micro- and nanoscale surface deposits whose morphology depends strongly on the electrochemical conditions [51]. These observations support the possibility that dissolution and redeposition processes contributed to the fine clustered structures observed in the present DES-treated samples. The coexistence of these two morphologies suggests a spatial variation in the relative importance of the degradation mechanisms. Within the UH area, mechanical cavitation loading appears to make a major contribution, while outside the directly exposed region, chemically driven dissolution and ultrasound-enhanced transport likely become relatively more important. Nevertheless, the two processes should not be regarded as spatially independent. Chemical attack was also evident within the cavitated region, while acoustic streaming and transported bubbles may have influenced areas beyond the UH area. This provides a plausible explanation for why the large gravimetric mass losses measured in the hydrated DES samples were not fully reflected by localized topographic damage beneath the UH.

5. Conclusions

This study presents an investigation of cavitation erosion caused by ultrasonic horn within different liquids, water-based and two deep eutectic solvents, containing two biopolymers chitin and chitosan. The results indicate that the composition of complex biopolymer-containing media influence cavitation dynamics and consequently impacts wear behavior of tested aluminum alloy specimen surface. Operating conditions of cavitation apparatus stayed constant throughout the experiments. In case of pure water, the material wear in terms of mass loss was the least pronounced. In water-based media with chitin and chitosan presence, material loss remained relatively low and was predominately localized within the area beneath the ultrasonic horn tip. No single physicochemical property could explain the observed erosion behavior,

indicating that cavitation response is governed by the combined effects of medium composition and properties.

Experiments with hydrated deep eutectic solvents exhibited different degradation behavior. Both [Ch]Cl:MA and [Ch]Cl:AA caused measurable aluminum dissolution without cavitation, while cavitation substantially accelerated material removal. Most severe degradation occurred within [Ch]Cl:AA, which also resulted in most spatially developed cavitation under the ultrasonic horn tip. Addition of chitin further increased the mass loss in [Ch]Cl:AA, whereas only a small effect was observed in [Ch]Cl:MA. These preliminary findings suggest that the influence of biopolymer may depend on the composition of the surrounding medium, although further experiments are required to confirm this behavior SEM and 3D topography revealed severe surface disruption within the cavitation-exposed region, while angular and step-like shape features, and surface deposits in DES-treated specimens indicated an additional contribution of chemical degradation. Consequently, mass loss in chemically reactive media should not be interpreted solely as mechanical cavitation erosion, but rather as cavitation-assisted material degradation resulting from coupled mechanical and chemical effects.

Since the experiments were performed using single replication, the observed differences between media should be regarded as preliminary and require confirmation through independent experimental replicates.

CRediT authorship contribution statement

Andraž Zupanc: Writing – review & editing, Writing – original draft, Visualization, Methodology, Investigation, Formal analysis, Data curation, Conceptualization. **Filipa A. Vicente:** Writing – review & editing, Methodology, Data curation. **Matevž Dular:** Writing – review & editing, Methodology, Funding acquisition. **Marko Hočevar:** Writing – review & editing, Funding acquisition. **Matej Hočevar:** Writing – review & editing, Formal analysis. **Odon Planinšek:** Writing – review & editing, Methodology, Formal analysis. **Mojca Zupanc:** Writing – review & editing, Writing – original draft, Methodology, Funding acquisition, Conceptualization. **Martin Petkovšek:** Writing – review & editing, Writing – original draft, Visualization, Supervision, Methodology, Investigation, Formal analysis, Data curation, Conceptualization.

Declaration of generative AI and AI-assisted technologies in the writing process

During the preparation of this manuscript, the authors used ChatGPT (OpenAI) to assist with English-language proofreading, grammar correction, and improvements in readability. The authors reviewed and edited the suggested changes and take full responsibility for the content of the published article.

Declaration of competing interest

The authors declare that they have no known competing financial interests or personal relationships that could have appeared to influence the work reported in this paper.

Acknowledgement

This work was supported by the Slovenian Research and Innovation Agency through Research Core Funding No. P2-0401, P2-0422, P1-0189 and Research Projects No. N2-0381, J2-70110, J2-60032 and J2-60051.

Appendix A. Supplementary data

Supplementary data to this article can be found online at https://doi.org/10.1016/j.wear.2026.207197.

Data availability

Data will be made available on request.

References

[1] J.-P. Franc, J.-M. Michel, Fundamentals of Cavitation, first ed., Kluwer Academic Publishers, 2004 https://doi.org/10.1007/1-4020-2233-6.
[2] Y. Benito, S. Arrojo, G. Hauke, P. Vidal, Hydrodynamic Cavitation as a low-cost AOP for Wastewater Treatment: Preliminary Results and a New Design Approach, 2005, https://doi.org/10.2495/WRM050501.
[3] K.S. Suslick, N.C. Eddingsaas, D.J. Flannigan, S.D. Hopkins, H. Xu, Extreme conditions during multibubble cavitation: sonoluminescence as a spectroscopic probe, in: Ultrason. Sonochem., Elsevier B.V., 2011, pp. 842–846, https://doi.org/10.1016/j.ultsonch.2010.12.012.
[4] H. Reese, S.-W. Ohl, C.-D. Ohl, Cavitation bubble induced wall shear stress on an elastic boundary, Phys. Fluids 35 (2023), https://doi.org/10.1063/5.0156507.
[5] B.J. Davidson, N. Riley, Cavitation microstreaming, J. Sound Vib. 15 (1971) 217–233, https://doi.org/10.1016/0022-460X(71)90536-0.
[6] C.E. Brennen, Cavitation and Bubble Dynamics, Cambridge University Press, 2013, https://doi.org/10.1017/CBO9781107338760.
[7] G.L. Chahine, C.T. Hsiao, Modelling cavitation erosion using fluid–material interaction simulations, Interface Focus 5 (2015) 1–21, https://doi.org/10.1098/rsfs.2015.0016.
[8] W. Ding, F. Hong, D. Ying, Y. Huang, S. Nawaz Khan, J. Jia, A comprehensive study on the effects of annular protrusion for cavitation intensification in Venturi tubes, Chem. Eng. J. 498 (2024) 155306, https://doi.org/10.1016/j.cej.2024.155306.
[9] A. Phillip, W. Lauterborn, Cavitation erosion by single laser-produced bubbles, J. Fluid Mech. 361 (1998) 75–116, https://doi.org/10.1017/S0022112098008738.
[10] M. Dular, M. Petkovšek, On the mechanisms of cavitation erosion – coupling high speed videos to damage patterns, Exp. Therm. Fluid Sci. 68 (2015) 359–370, https://doi.org/10.1016/j.expthermflusci.2015.06.001.
[11] K.S. Kaaviya, V. Nithyalakshmi, V. Perasiriyan, R. Marx Nirmal, Validation of ultrasound cavitation at 20 kHz and 40 kHz frequency in an ultrasound Bath using the aluminium foil corrosion Test, Madras Agric. J. 111 (2024), https://doi.org/10.29321/MAJ.10.600002.
[12] M. Dular, G.E.B. Montalvo, M. Hočevar, L. Novak, C.D. Ohl, M. Petkovsek, Questioning the ASTM G32-16 (stationary specimen) standard cavitation erosion test, Ultrason. Sonochem. 107 (2024) 106930, https://doi.org/10.1016/j.ultsonch.2024.106930.
[13] S. Sun, P. Wu, P. Guo, H. Nan, T. Wang, Effect of ultrasonic amplitude on cavitation erosion characteristics of hydraulic turbine materials, Phys. Fluids 37 (2025), https://doi.org/10.1063/5.0252423.
[14] T. Volkov-Husovic, S. Martinovic, A. Alil, M. Vlahovic, B. Dimitrijevic, I. Ivanic, V. Pavkov, Comparative investigation of ultrasonic cavitation erosion for two engineering materials, J. Min. Metall. B Metall. 60 (2024) 295–304, https://doi.org/10.2298/JMMB240118018V.
[15] J. Zhao, L. Ning, J. Zhu, Y. Li, Investigation on ultrasonic cavitation erosion of aluminum–titanium alloys in sodium chloride solution, Crystals 11 (2021) 1299, https://doi.org/10.3390/cryst11111299.
[16] I. Tzanakis, G.S.B. Lebon, D.G. Eskin, K.A. Pericleous, Characterizing the cavitation development and acoustic spectrum in various liquids, Ultrason. Sonochem. 34 (2017) 651–662, https://doi.org/10.1016/j.ultsonch.2016.06.034.
[17] S. Safaei, C. Mehring, Effect of dissolved carbon dioxide on cavitation in a circular orifice, Fluid 9 (2024) 41, https://doi.org/10.3390/fluids9020041.
[18] C. Luo, J. Gu, X. Xu, P. Ma, H. Zhang, X. Ren, Impact of solid particles on cavitation behaviors and laser-induced degradation in aqueous suspension, Ultrason. Sonochem. 76 (2021) 105632, https://doi.org/10.1016/j.ultsonch.2021.105632.
[19] E. Loranger, M. Paquin, C. Daneault, B. Chabot, Comparative study of sonochemical effects in an ultrasonic bath and in a large-scale flow-through sonoreactor, Chem. Eng. J. 178 (2011) 359–365, https://doi.org/10.1016/j.cej.2011.10.021.
[20] S. Biswas, T.U. Rashid, Effect of ultrasound on the physical properties and processing of major biopolymers—a review, Soft Matter 18 (2022) 8367–8383, https://doi.org/10.1039/D2SM01339H.
[21] A. Zupanc, J. Ortar, D. Pahovnik, N.Z. Logar, B. Stres, A. Šmid, M. Zupanc, M. Petkovšek, E. Žagar, Preparation of low molecular weight chitosan through hydroxyl radicals generated via hydrodynamic cavitation, Ultrason. Sonochem. 123 (2025) 107688, https://doi.org/10.1016/j.ultsonch.2025.107688.
[22] N. Ozel, M. Elibol, Chitin and chitosan from mushroom (Agaricus bisporus) using deep eutectic solvents, Int. J. Biol. Macromol. 262 (2024) 130110, https://doi.org/10.1016/j.ijbiomac.2024.130110.
[23] Y. Wu, Y. Huang, Y. Zhou, X. Ren, F. Yang, Degradation of chitosan by swirling cavitation, Innov. Food Sci. Emerg. Technol. 23 (2014) 188–193, https://doi.org/10.1016/j.ifset.2014.02.001.
[24] Y. Huang, Y. Wu, W. Huang, F. Yang, X.E. Ren, Degradation of chitosan by hydrodynamic cavitation, Polym. Degrad. Stabil. 98 (2013) 37–43, https://doi.org/10.1016/j.polymdegradstab.2012.11.001.
[25] J. Yan, J. Xu, S. Ai, K. Zhang, F. Yang, Y. Huang, Degradation of chitosan with self-resonating cavitation, Arab. J. Chem. 13 (2020) 5776–5787, https://doi.org/10.1016/j.arabjc.2020.04.015.
[26] J. Yan, S. Ai, F. Yang, K. Zhang, Y. Huang, Study on mechanism of chitosan degradation with hydrodynamic cavitation, Ultrason. Sonochem. 64 (2020), https://doi.org/10.1016/j.ultsonch.2020.105046.

[27] V. Garbin, Bubble dynamics in complex fluids, Phys. Rev. Fluids 11 (2026) 010502, https://doi.org/10.1103/hj5m-fcvt.
[28] R. Azadi, D.S. Nobes, Hydrodynamic cavitation reduction in semidilute turbulent polymer solution flows, J. Fluid Mech. 952 (2022) A29, https://doi.org/10.1017/jfm.2022.910.
[29] F.A. Vicente, M. Huš, B. Likozar, U. Novak, Chitin deacetylation using deep eutectic solvents: ab initio -Supported process optimization, ACS Sustain. Chem. Eng. 9 (2021) 3874–3886, https://doi.org/10.1021/acssuschemeng.0c08976.
[30] A.P. Abbott, D. Boothby, G. Capper, D.L. Davies, R.K. Rasheed, Deep eutectic solvents formed between choline Chloride and carboxylic acids: versatile alternatives to ionic liquids, J. Am. Chem. Soc. 126 (2004) 9142–9147, https://doi.org/10.1021/ja048266j.
[31] D.O. Abranches, J.A.P. Coutinho, Everything you wanted to know about deep eutectic solvents but were afraid to be told, Annu. Rev. Chem. Biomol. Eng. 14 (2023) 141–163, https://doi.org/10.1146/annurev-chembioeng-101121-085323.
[32] J. Wang, C. Teng, L. Yan, Applications of deep eutectic solvents in the extraction, dissolution, and functional materials of chitin: research progress and prospects, Green Chem. 24 (2022) 552–564, https://doi.org/10.1039/D1GC04340D.
[33] K. Morgan, C. Conway, S. Faherty, C. Quigley, A comparative analysis of conventional and deep eutectic solvent (DES)-Mediated strategies for the extraction of chitin from Marine Crustacean shells, Molecules 26 (2021) 7603, https://doi.org/10.3390/molecules26247603.
[34] B. Jacobson, S. Li, P. Daly, C.E. Elgar, A.P. Abbott, A. Feeney, P. Prentice, Observation of cavitation dynamics in viscous deep eutectic solvents during power ultrasound sonication, Faraday Discuss. 253 (2024) 458–477, https://doi.org/10.1039/D4FD00031E.
[35] Y. Liu, Z.-Y. Zheng, Z.-B. He, T.-B. Zeng, L. Wang, W.-H. Cai, H. Qi, Interactions between cavitation bubbles and free surfaces of Non-Newtonian polymer solutions, Phys. Fluids 36 (2024), https://doi.org/10.1063/5.0226255.
[36] A. Pandit, A. Indurkar, C. Deshpande, R. Jain, P. Dandekar, A systematic review of physical techniques for chitosan degradation, Carbohydr. Polym. Technol. Appl. 2 (2021) 100033, https://doi.org/10.1016/j.carpta.2021.100033.
[37] H. Zong, G. Qu, F. Yang, F. Ye, Y. Liu, X. Xu, X. He, Q. Lu, S. Sun, Ultrasound-Assisted deep eutectic solvent-based green extraction of flavonoids from honeysuckle: optimization and mechanistic insights into α-Amylase inhibition, Foods 15 (2025) 10, https://doi.org/10.3390/foods15010010.
[38] V.N. Davydova, I.M. Yermak, The conformation of Chitosan molecules in aqueous solutions, Biophysics 63 (2018) 501–511, https://doi.org/10.1134/S000635091804005X.
[39] E.L. Smith, A.P. Abbott, K.S. Ryder, Deep eutectic solvents (DESs) and their applications, Chem. Rev. 114 (2014) 11060–11082, https://doi.org/10.1021/cr300162p.
[40] T. El Achkar, H. Greige-Gerges, S. Fourmentin, Basics and properties of deep eutectic solvents: a review, Environ. Chem. Lett. 19 (2021) 3397–3408, https://doi.org/10.1007/s10311-021-01225-8.
[41] Y. Deng, H. Xi, Z. Gu, X. Yan, Cavitation-driven bubble evolution and load mechanisms in particle-wall multiphase interactions, Ultrason. Sonochem. 120 (2025) 107461, https://doi.org/10.1016/j.ultsonch.2025.107461.
[42] I.M. Pateli, D. Thompson, S.S.M. Alabdullah, A.P. Abbott, G.R.T. Jenkin, J. M. Hartley, The effect of pH and hydrogen bond donor on the dissolution of metal oxides in deep eutectic solvents, Green Chem. 22 (2020) 5476–5486, https://doi.org/10.1039/D0GC02023K.
[43] E.I. Ahmed, K.S. Ryder, A.P. Abbott, Corrosion of iron, nickel and aluminium in deep eutectic solvents, Electrochim. Acta 397 (2021) 139284, https://doi.org/10.1016/j.electacta.2021.139284.
[44] N. Kim, W. Yang, J. Amphlett, D. Kang, Y. Lee, J.J. Kim, H.J. Ryu, S. Choi, Surface decontamination of protective duplex oxide layers on stainless steel waste using deep eutectic solvents, J. Hazard Mater. 425 (2022) 128000, https://doi.org/10.1016/j.jhazmat.2021.128000.
[45] O.M. Gradov, I.V. Zinov'eva, YuA. Zakhodyaeva, A.A. Voshkin, Kinetics of ultrasound-assisted dissolution of a LiCoO2 powder in the deep eutectic solvent choline Chloride–Sulfosalicylic acid, Theor. Found. Chem. Eng. 56 (2022) 997–1002, https://doi.org/10.1134/S0040579522060069.
[46] P. Hunt, J.M. Hartley, M.A. Rabeea, A.P. Abbott, C.E. Elgar, Electrochemical etching of metals and minerals using ultrasound in deep eutectic solvents, Ultrason. Sonochem. 119 (2025) 107403, https://doi.org/10.1016/j.ultsonch.2025.107403.
[47] E. Daskalopoulou, P. Hunt, C.E. Elgar, M. Yang, A.P. Abbott, J.M. Hartley, Overcoming passivation through improved mass transport in dense ionic fluids, Faraday Discuss. 253 (2024) 329–342, https://doi.org/10.1039/D4FD00030G.
[48] M. Zhang, X. Zhao, S. Tang, K. Wu, B. Wang, Y. Liu, Y. Zhu, H. Lu, B. Liang, Structure–properties relationships of deep eutectic solvents formed between choline chloride and carboxylic acids: experimental and computational study, J. Mol. Struct. 1273 (2023) 134283, https://doi.org/10.1016/j.molstruc.2022.134283.
[49] O. Adarraga, C. Agustín-Sáenz, I. Bustero, F. Brusciotti, Superhydrophobic and oleophobic microtextured aluminum surface with long durability under corrosive environment, Sci. Rep. 13 (2023) 1737, https://doi.org/10.1038/s41598-023-28587-z.
[50] C. Liu, J. Wang, Z. Zhang, E.-H. Han, Studies on corrosion behaviour of low carbon steel canister with and without γ-irradiation in China's HLW disposal repository, Corrosion Engineering, Sci. Technol. 52 (2017) 136–140, https://doi.org/10.1080/1478422X.2017.1348762.
[51] V.S. Cvetković, N.M. Vukićević, N. Jovićević, J.S. Stevanović, J.N. Jovićević, Aluminium electrodeposition under novel conditions from AlCl3–urea deep eutectic solvent at room temperature, Trans. Nonferrous Met. Soc. China 30 (2020) 823–834, https://doi.org/10.1016/S1003-6326(20)65257-8.